International Journal of Mining Science and Technology xxx (xxxx) xxx

Contents lists available at ScienceDirect

International Journal of Mining Science and Technology

journal homepage: www.elsevier.com/locate/ijmst

A system for underground road condition monitoring

Max Åstrand [a,b,*], Erik Jakobsson [c,d], Martin Lindfors [d], John Svensson [d,e]

[a] KTH Royal Institute of Technology, SE-100 44 Stockholm, Sweden
[b] ABB Corporate Research, SE-722 26 Västerås, Sweden
[c] Epiroc, SE-701 91 Örebro, Sweden
[d] Linköping University, SE-581 83 Linköping, Sweden
[e] Boliden Mines, SE-936 32 Boliden, Sweden

ARTICLE INFO

Article history:
Received 1 October 2019
Received in revised form 27 January 2020
Accepted 14 April 2020
Available online xxxx

Keywords:
Localization
Road condition monitoring
Scheduling
Underground mining

ABSTRACT

Poor road conditions in underground mine tunnels can lead to decreased production efficiency and increased wear on production vehicles. A prototype system for road condition monitoring is presented in this paper to counteract this. The system consists of three components i.e. localization, road monitoring, and scheduling. The localization of vehicles is performed using a Rao-Blackwellized extended particle filter, combining vehicle mounted sensors with signal strengths of WiFi access points. Two methods for road monitoring are described: a Kalman filter used together with a model of the vehicle suspension system, and a relative condition measure based on the power spectral density. Lastly, a method for taking automatic action on an ill-conditioned road segment is proposed in the form of a rescheduling algorithm. The scheduling algorithm is based on the large neighborhood search and is used to integrate road service activities in the short-term production schedule while minimizing introduced production disturbances. The system is demonstrated on experimental data collected in a Swedish underground mine.

1. Introduction

Underground mine roads can span several hundred kilometers, and the road surface quality is important for the mining operation. Roads wear over time and a too ill-conditioned road may lead to increased wear on vehicles and limit the pace of production. In this work, a prototype method for localizing vehicles and monitoring road quality without any additional in-mine infrastructure is developed. A way of incorporating the road quality information in the short-term production schedule is also introduced. The joint proof-of-concept system, bringing together different scientific fields, is tested on data collected in the Boliden Kankberg gold mine in Sweden.

The main idea is to equip vehicles with sensors that gather data during normal operations. The data can then be used for (1) localizing the vehicles with respect to a mine-wide map, (2) estimating the quality of road surface at the vehicle location, and (3) accounting for the road quality information in the currently operating short-term production schedule. The system is thus composed of three logical parts i.e. localization, condition monitoring, and scheduling, all of which will briefly be introduced.

Localization consists of estimating the position of an object using information e.g. sensor measurements, object dynamics and maps. Most available systems for underground mine localization depend either on external infrastructure e.g. ultra-wideband networks, or expensive onboard sensors e.g. LIDARs [1,2]. In this work, a vehicle in a mine is localized using several inexpensive sources of information including an inertial measurement unit, wheel speed sensors and received signal strength indications (RSSI) from already present WiFi access points. A dynamical model of the vehicle and sensor models for all sensors are designed. A Rao-Blackwellized extended particle filter is then proposed to localize the vehicle.

Condition monitoring is a broad field in signal processing that tries to estimate the condition of an asset given a limited number of signals. In this work, the goal is to characterize the road condition, one of the main causing factors for mine vehicle condition deterioration. Since many different types of vehicles use the mine roads, it is of importance to find a measure not unique to a specific vehicle. The road profile is such a measure which is well known for allowing estimation of various measures of damage for different types of vehicles [3]. The commonly known quarter car model is typically used to simulate vehicle dynamics given a road profile.

* Corresponding author at: KTH Royal Institute of Technology, SE-100 44 Stockholm, Sweden.
E-mail address: max.astrand@se.abb.com (M. Åstrand).

https://doi.org/10.1016/j.ijmst.2020.04.006
2095-2686/

Please cite this article as: M. Åstrand, E. Jakobsson, M. Lindfors et al., A system for underground road condition monitoring, International Journal of Mining Science and Technology, https://doi.org/10.1016/j.ijmst.2020.04.006

Herein, the quarter car model is used backwards: given the vehicle dynamics estimate the road profile. A power spectral density measure is also considered, which is used as a general roughness measure of the road [4].

Short-term scheduling is the process of timetabling and allocating resources (machines and workers) to individual mining tasks in order to achieve a predetermined production goal. Recently, efforts have been made to automate the construction of short-term schedules by e.g. a decision-support algorithm for scheduling the production cycle in a Finnish gold mine, and a mixed-integer linear programming for scheduling a German room-and-pillar potash mine [5,6]. In this work, the production schedule is automatically adjusted for road service activities, which are often ad-hoc tasks and are not a part of the production schedule. However, they may affect the current schedule by limiting access to production areas near the road being worked on. These disturbances are accommodated by rescheduling using large neighborhood search (LNS), aiming at creating a new schedule that avoids shop floor nervousness i.e. minimizing the number of required schedule changes [7,8].

2. Theory

2.1. Localization

This section outlines the design of the localization method including a dynamical model, a measurement model and a Rao-Blackwellized extended particle filter (RBEPF). The sensors used for the localization are:

(1) A 3-axis gyro mounted in the vehicle with measurements, called y^{GYRO}.
(2) A 3-axis accelerometer mounted in the vehicle, called y^{ACC}.
(3) A wheel axle speed sensor from OBD, called y^{WSS}.
(4) A RSSI sensor measuring the signal strength of WiFi access points, called y^{RSS}.

In addition, a node graph of the mine and locations of the WiFi access points are available.

2.1.1. Dynamical model

A dynamical model describes how a system evolves over time. Our dynamical model describes the movement of a vehicle inside an underground tunnel. The states of the dynamical model are:

(1) Position in X, Y, and Z directions (north, west, and up), $\boldsymbol{x} = [x^x, x^y, x^z]^{\mathrm{T}}$.
(2) Velocity in the same coordinates, $\boldsymbol{v} = [v^x, v^y, v^z]^{\mathrm{T}}$.
(3) Roll, pitch and yaw Euler angles collected, respectively, in the angle vector $\boldsymbol{\eta} = [\phi, \theta, \psi]^{\mathrm{T}}$.
(4) Local roll, pitch and yaw angular velocities, $\boldsymbol{\omega} = [\omega^{\phi}, \omega^{\theta}, \omega^{\psi}]^{\mathrm{T}}$.
(5) Yaw angular gyro bias, $b^{\omega\psi}$.

The dynamical model can be formulated as

$$\dot{\mathbf{x}} = \mathbf{v} \tag{1}$$

$$\dot{\mathbf{v}} = R^{\mathrm{B}\to\mathrm{W}}(\eta)v + \omega^{\mathbf{v}} \tag{2}$$

$$\dot{\eta} = T(\eta)\omega \tag{3}$$

$$\dot{\omega} = w^{\omega} \tag{4}$$

$$\dot{\mathbf{b}}^{\omega^{\psi}} = w^{b,\omega^{\psi}} \tag{5}$$

The body-to-world and world-to-body rotation matrices, $R^{B\to W}(\boldsymbol{\eta})$ and $R^{W\to B}(\boldsymbol{\eta})$, are used to convert between the world (global) and body (local) coordinate systems, and the matrix $T(\boldsymbol{\eta})$ translates local to global angular velocities. See [9] for details.

2.1.2. Measurement models

The measurements, which include analytic states i.e. estimated by (extended) Kalman filters, must have Gaussian noise models to be suitable for the RBEPF. The measurement equations for the analytic states are

$$y^{\mathrm{ACC}} = R^{\mathrm{W}\to\mathrm{B}}(\eta)[0 \quad 0 \quad g]^{\mathrm{T}} + e^{\mathrm{ACC}} \tag{6}$$

$$y^{\mathrm{GYRO}} = \omega + e^{\mathrm{GYRO}} \tag{7}$$

$$\begin{bmatrix} y^{\mathrm{WSS}} & 0 & 0 \end{bmatrix}^{\mathrm{T}} = R^{\mathrm{W}\to\mathrm{B}}(\eta)\mathbf{v} + e^{\mathrm{WSS}} \tag{8}$$

where the noises e^{ACC}, e^{GYRO}, and e^{WSS} are Gaussian and zero mean. Eq. (8) models both the wheel axle speed sensor measurement (first row of the matrix equation) and the kinematic constraint forcing the vehicle not to move laterally or vertically (second and third rows).

The distribution of the availability of a measurement, a^{RSS}, along with the value of measurement y^{RSS} from the access point (AP) position x^{RSS}, is modeled as

$$p(y^{\mathrm{RSS}}, a^{\mathrm{RSS}}|\boldsymbol{x}) = \begin{cases} 1 - P_a^{\mathrm{RSS}}(\mathbf{x}, \mathbf{x}^{\mathrm{RSS}}), a^{\mathrm{RSS}} = 0 \\ P_a^{\mathrm{RSS}}(\mathbf{x}, \mathbf{x}^{\mathrm{RSS}}) p_y^{\mathrm{RSS}}(y^{\mathrm{RSS}}|\mathbf{x}, \mathbf{x}^{\mathrm{RSS}}), a^{\mathrm{RSS}} = 1 \end{cases} \tag{9}$$

where P_a^{RSS} is the probability of measuring the AP; and p_y^{RSS} the distribution of the measured AP signal strength y^{RSS}. To model the received signal strength, the distance $d(\boldsymbol{x}^{\mathrm{RSS}}, \boldsymbol{x})$ along the mine tunnel from the AP to the current position is calculated. The predicted RSS is modeled as

$$\widehat{RSS} = RSS_0 - \alpha \cdot 10\log_{10} d(\mathbf{x}^{\mathrm{RSS}}, \mathbf{x}) \tag{10}$$

where RSS_0 is the received signal strength at 1 m; and α the decay rate in signal strength. The measurement probability $P_a^{\mathrm{RSS}}(\mathbf{x}, \psi, \mathbf{x}^{\mathrm{RSS}})$ is then modeled as a perturbed logistic function.

$$p_a^{\mathrm{RSS}}(\mathbf{x}, \psi, \mathbf{x}^{\mathrm{RSS}}) = \beta_\infty + (\beta_0 - \beta_\infty) / \left[1 + \exp\left(k\left(\widehat{RSS} - RSS_{\mathrm{thres}}\right)\right)\right] \tag{11}$$

where β_0 and β_∞ are the probabilities of getting an RSS measurement at distance 0 and distance ∞, respectively; RSS_{thres} the RSS value when the measurement probability is in the midpoint $(\beta_0 + \beta_\infty)/2$; and k the scaling parameter determining the speed of the change.

The distribution of the measurement value is selected as a Student's t distribution.

$$p_y^{\mathrm{RSS}}(y^{\mathrm{RSS}}|\mathbf{x}, \psi, \mathbf{x}^{\mathrm{RSS}}) = \mathrm{S}\left(y^{\mathrm{RSS}} \middle| \hat{RSS}, \sigma_{\mathrm{RSS}}, \nu_{\mathrm{RSS}}\right) \tag{12}$$

where the scale parameter σ_{RSS} and degree of freedom parameter ν_{RSS} are tuning parameters. This choice was made in order to handle outliers in the RSS measurements [10].

In order to constrain the vehicle to the mine tunnel, a virtual measurement

$$p(y^{\mathrm{wall}}|x) = N(y^{\mathrm{wall}}|d_{\mathrm{map}}(\mathbf{x}), \sigma^{\mathrm{wall}}) \tag{13}$$

is adjoined where $d_{\mathrm{map}}(\boldsymbol{x})$ is the shortest distance from the current position to the mine tunnel; and $y^{\mathrm{wall}} = 0$.

2.1.3. Rao-Blackwellized extended particle filter

Given the model described above, an RBEPF is applied. The model is discretized using Euler-Maruyama discretization. The

Please cite this article as: M. Åstrand, E. Jakobsson, M. Lindfors et al., A system for underground road condition monitoring, International Journal of Mining Science and Technology, https://doi.org/10.1016/j.ijmst.2020.04.006

states are partitioned between the states $x^p = [\boldsymbol{x}^T, \psi]^T$, which are estimated using a particle filter, and the states $x^k = [\boldsymbol{v}^T, \phi, \theta, \boldsymbol{\omega}^T, b^{\omega\psi}]^T$, which are estimated using extended Kalman filters conditionally on the particle state x^p. For further information on the RBEPF, consult e.g. [11].

2.2. Condition monitoring

A known road profile enables many types of calculations, such as wear for different types of vehicles and translation to e.g. the international road roughness index [12]. To obtain the road profile a quarter car model together with a Kalman filter is proposed.

2.2.1. Quarter car Kalman filter model

A quarter car model is typically used to simulate vehicle dynamics using a known road profile. In this work the model is used in the opposite direction, by recreating an unknown road profile using the response dynamics measured on the vehicle. Accelerometers measure the accelerations of both the unsprung mass i.e. the suspension and wheels of the car, and the sprung mass i.e. the parts of the car supported by the suspension. Fig. 1 shows the common quarter car model.

The quarter car model used is given as

$$\dot{\mathbf{x}}_s = \mathbf{v}_s \tag{14}$$

$$\dot{\mathbf{v}}_s = -(k_s/m_s)\mathbf{x}_s - (c_s/m_s)\mathbf{v}_s + (k_s/m_s)\mathbf{x}_u + (c_s/m_s)\mathbf{v}_u \tag{15}$$

$$\dot{\mathbf{x}}_u = \mathbf{v}_u \tag{16}$$

$$\dot{\mathbf{v}}_u = (k_s/m_u)\mathbf{x}_s + (c_s/m_u)\mathbf{v}_s - ((k_t + k_s)/m_u)\mathbf{x}_u - (c_s/m_u)\mathbf{v}_u + (k_t/m_u)\mathbf{x}_0 \tag{17}$$

$$\dot{\mathbf{x}}_0 = \mathbf{v}_0 - a_0\mathbf{x}_0 \tag{18}$$

$$\dot{\mathbf{v}}_0 = -b_0\mathbf{x}_0 \tag{19}$$

where $\boldsymbol{x}$ denotes the position; $\boldsymbol{v}$ the velocity; and the subscripts s, u, 0 the sprung mass, unsprung mass and road, respectively. It is assumed that the tire damping coefficient $c_t = 0$. The tuning constants a_0 and b_0 affect the low pass filtering of the road profile. Let the state vector be given as

$$x = [\mathbf{x}_s, \mathbf{v}_s, \mathbf{x}_u, \mathbf{v}_u, \mathbf{x}_0, \mathbf{v}_0]^T \tag{20}$$

and the measurement as

$$y = [\mathbf{a}_s, \mathbf{a}_u]^T \tag{21}$$

where $\boldsymbol{a}_s$ and $\boldsymbol{a}_u$ are the acceleration of the sprung and unsprung mass, respectively. The model can then be written on state-space form as

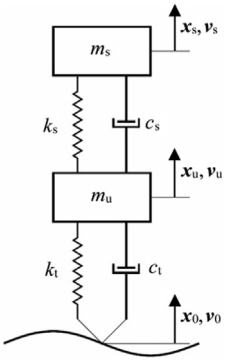

Fig. 1. The quarter car model.

$$\dot{x} = Ax + v_k \tag{22}$$

$$y = Cx + e_k \tag{23}$$

where A is given by Eqs. (14)–(19). in the quarter car model and C by Eqs. (15) and (17).

Considering this structure, where $f(x_k) = Ax_k$ and $h(x_k) = Cx_k$ are linear in x_k, and $v_k \sim N(0,Q)$ and $e_k \sim N(0,R)$ are jointly Gaussian, the road profile can then be estimated using a Kalman filter [13,14].

2.2.2. Power spectral density

The power spectral density (PSD) describes the amount of energy present in a signal for each frequency component. For this work, the Welch method is used with a Hamming window of 50 samples [15]. The PSD is closely related to both the roughness of the road surface and the durability of the vehicle, making the average PSD a good one-value-measure of road condition.

2.3. Scheduling

In this section, a scheduling algorithm for creating short-term mine schedules will first be presented. Then, a method to restore feasibility to a schedule that is disturbed by a road service activity is introduced.

2.3.1. A constraint-based mine scheduling model

Short-term scheduling can be automated by using constraint programming (CP), a method that exploits the structure of the scheduling problem to quickly produce feasible schedules [16].

All mining tasks are modeled using conditional task variables [17]. This means that each task i on face f (the production area) is associated with a tuple $s^f_{ir}, e^f_{ir}, d^f_{ir}, o^f_{ir}$, representing start time, end time, task duration, and execution status, respectively ($s^f_{ir} + d^f_{ir} = e^f_{ir}$). The index i ranges from 1 to $|A^f|$, where A^f is the set of all activities on face f. The binary execution status o^f_{ir} contains the conditional aspect, meaning that o^f_{ir} is nonzero if and only if the task i is scheduled on machine r.

Considering mining methods that follow a drill-and-blast mining cycle, the mining sequence can be explicitly enforced by

$$s^f_{ir} + d^f_{ir} < s^f_{i+1,r'} \;\; \forall(f,i,r,r') \text{s.t. } r,r' \in M_{c(a^f_i)} \tag{24}$$

where $c\left(a^f_i\right)$ is the activity type of task a^f_i; and $M_{c(a^f_i)}$ the set of all machines eligible to process that task.

Blasting takes place during blast windows. Some tasks can be split over a blast window while others (e.g. activities involving concrete) cannot. This means that the problem consists of a mix of interruptible and non-interruptible tasks. To model this, the task duration is treated as variable rather than constant. Denote the set of non-interruptible tasks by A^f_{NI}. The duration of these tasks is constrained to be the nominal duration D^f_i.

$$d^f_{ir} = D^f_{ir} \;\; \forall(i,f) \text{s.t. } a^f_i \in A^f_{NI} \tag{25}$$

However, for interruptible tasks auxiliary variables p^f_{ir} need to be introduced, indicating whether the task a^f_i is scheduled so that it starts before a blast window and ends after. This variable duration, dependent on where in time a task is scheduled, can be modeled by

$$p^f_{ir} = \sum_k \left(s^f_{ir} < s_{b_k}\right) * \left(s^f_{ir} + d\left(a^f_i\right) > s_{b_k}\right) \tag{26}$$

$$d^f_{ir} = D^f_i + p^f_{ir} * d_b \;\; \forall(i,f) \tag{27}$$

Please cite this article as: M. Åstrand, E. Jakobsson, M. Lindfors et al., A system for underground road condition monitoring, International Journal of Mining Science and Technology, https://doi.org/10.1016/j.ijmst.2020.04.006

where d_b is the length of the blast window; and s_{bk} the start time of blast window k.

Lastly, each face and each machine is a disjunctive resource i.e. a machine can only process one task at a given time, and, due to the confined environment, only one machine can be simultaneously present at a given face. This is captured for both faces and machines by the global **unary** constraint.

$$\textbf{unary}\left(\left\{\left[s_{ir}^f, d_{ir}^f, o_{ir}^f\right] | \forall r, i\right\}\right) \ \forall f \tag{28}$$

$$\textbf{unary}\left(\left\{\left[s_{ir}^f, d_{ir}^f, o_{ir}^f\right] | \forall f, i\right\}\right) \ \forall r \tag{29}$$

A CP solver alternates between search and model inference. For more details on the model see [18], where the search heuristic is also presented in detail.

2.3.2. Rescheduling using LNS

Large neighborhood search (LNS) can be used to restore the feasibility to a constructed schedule containing a resource conflict. The idea is to seek for schedules by exploring a neighborhood around the original schedule. A neighborhood is defined as the set of schedules possible to produce by relaxing (restoring the domain) of some assigned variables. Within this restricted neighborhood, a feasible assignment of the relaxed variables might be found.

Road service may affect the availability of faces by blocking access roads. Thus, tasks that have started on these faces may continue, but no new tasks can start there. The disturbance hence manifests itself as unavailability of faces during certain time windows, described by a logical statement as

$$s_{ir}^f < t_{\text{start}} \vee s_{ir}^f > t_{\text{end}} \quad \forall (i, r) \ and \ f \in \hat{F} \tag{30}$$

Here $\hat{F}$ holds all faces that are affected by the road service activity, and the disturbance takes place between t_{start} and t_{end}. In general, several types of relaxations can be useful e.g. face-based (all tasks scheduled on a specific face are relaxed) or machine-based (all tasks that require a certain machine type are relaxed). However, for this type of disturbance a time-based relaxation neighborhood is employed meaning that all task variables $s_{ir}^f, e_{ir}^f, d_{ir}^f, o_{ir}^f$ corresponding to tasks scheduled between t_{start} and t_{end} are relaxed. The time-based relaxation is fixed around the midpoint of the disturbance, $t_{\text{start}} + (t_{\text{end}} - t_{\text{start}})/2$, but the width of the relaxation window grows as the computation progresses. Starting with a narrow relaxation which is eventually broadened means that once a feasible solution is found, it is likely to be similar to the original schedule.

3. Results

To collect the necessary data, a pick-up truck is instrumented with two 3DOF ADXL345 accelerometers, one 3DOF L3GD20 gyroscope, and an OBD2-interface to read wheel speed messages on the CAN-bus of the vehicle. One accelerometer is mounted on the wheel suspension, while the other one is mounted together with the gyroscope on the dashboard. All measurements are collected using a Raspberry Pi 3, which also provides signal strength measurements of WiFi connections to nearby access points.

3.1. Localization

Localization parameters were selected by using the calibration data, through physical reasoning, and by hand-tuning. See Table 1. The remainder of the states did not need to be tuned since they are measured by the IMU or OBD sensors.

It was found that initializing the filter with a computationally feasible number of particles (1000) spread throughout the mine produced poor results. Therefore, an initialization routine based on the RSS model found in Eq. (10) was used. This approach was found to perform better, although the RSS measurement model appeared to be imperfect, making positioning more difficult. An example of the expected and actual RSS measurements is shown in Figs. 2 and 3. It can be seen that the measurement model captures some relationship between the measurement and the position, albeit not perfectly. The model for the probability of receiving measurements from an access point during the same run, depicted in Fig. 2, appears to match the actual outcome.

After the initial state is estimated, the filter is run. An example trajectory can be seen in Fig. 4b and c, where the authors localize the vehicle traveling down the main ramp in the mine by using only onboard IMU and measured WiFi signal strength. It appears from Fig. 4b and c that the vehicle is localized close to its real path. As validation, the corresponding posterior mean and standard deviation of the states are illustrated in Fig. 4a.

3.2. Road monitoring

The quarter car Kalman approach is intended to estimate the road profile given the acceleration inputs from the two masses in the model. The concept was evaluated using both simulated and experimental data.

Measuring the real road profile in the mine requires specialized equipment unavailable in this project. Therefore, a synthetic dataset including both accelerations and ground truth road profile was generated by using a quarter car model in the conventional way i.e. to generate accelerations from a known road profile. To incorporate some uncertainty in the synthetic data, Gaussian noise with a signal-to-noise ratio of 1–10 was added to the generated acceleration signals.

Using the synthetic data, Fig. 5 shows that the condition monitoring algorithm is able to capture the high frequency oscillations of all the estimated signals. Signals denoted by "hat" are the esti-

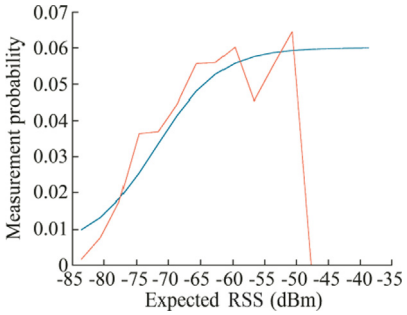

Fig. 2. Expected probability (blue) and actual frequency (orange) of WiFi measurements as a function of expected received signal strength from the test drive.

Table 1
Parameter values.

M	σ^{v^X, v^Y}	σ^{v^Z}	$\sigma^{\omega^\phi, \omega^\theta}$	σ^{ω^ψ}	σ^{b, ω^ψ}	$\sigma^{y^{ACC}}$	$\sigma^{y^{GYRO}}$	$\sigma^{y^{WSS}}$	$\sigma^{kinematic}$	σ^{wall}	σ_{RSS}	v_{RSS}	α	β_∞	k	RSS_{thres}
1000	0.5	0.2	0.2	0.2	10^{-5}	2	0.1	0.1	0.001	5	10	3	1.73	0.005	0.2	−72

Please cite this article as: M. Åstrand, E. Jakobsson, M. Lindfors et al., A system for underground road condition monitoring, International Journal of Mining Science and Technology, https://doi.org/10.1016/j.ijmst.2020.04.006

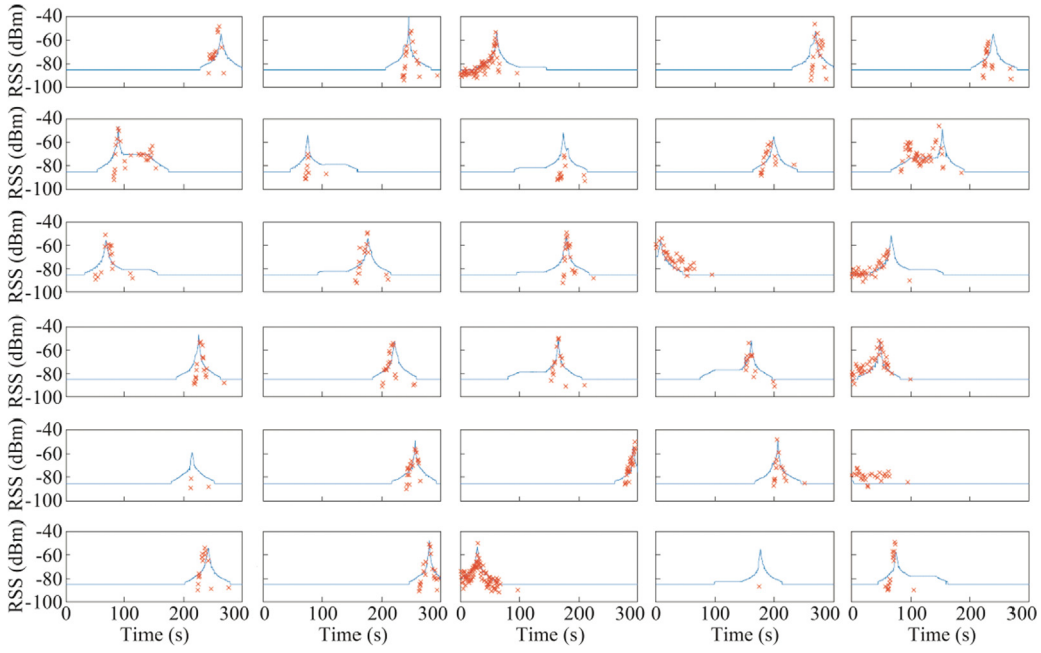

Fig. 3. Expected WiFi measurement strength (blue) and actual measurement strength (orange) from a test drive.

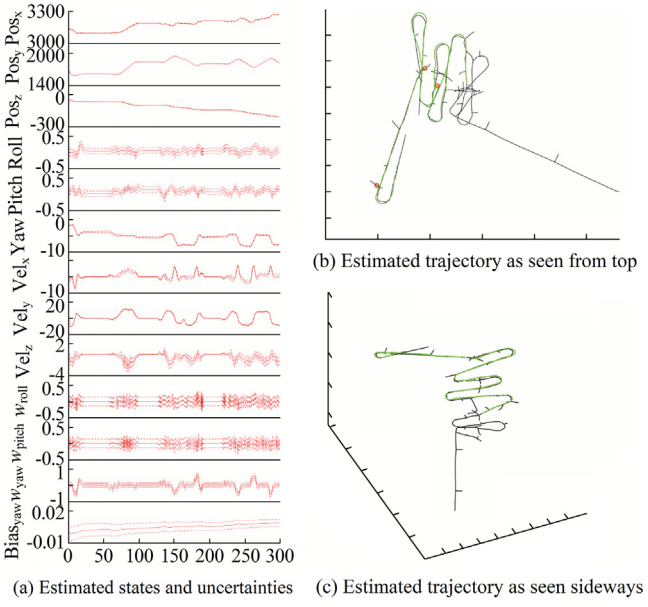

Fig. 4. (a) shows estimated states. It can be seen that the bias varies over the trajectory. During the descent, the temperature increases from negative to positive degrees Celsius, which is hypothesized to yield a change in gyro bias (yaw gyro bias is estimated dynamically); (b) and (c) hold the localized trajectory (green) of a pick-up driving down the ramp, with the mine map in black. Vehicle stops due to traffic are encircled in red. The trajectory starts at the mine entrance, i.e. top left in (c).

mations made using both acceleration signals, while signals denoted by "hat_s_only" use only the body mounted accelerometer. Blue lines are the ground truth data. The divergence between true and simulated results is due to drift issues since an integration is required to obtain position from the acceleration signals. This mainly concerns the position estimate x_s, x_u, x_0 and is most prominent for x_0 i.e. the road surface estimate. Using both accelerometers yields slightly better results than using only the body mounted accelerometer, but both approaches give a decent representation of the road surface x_0.

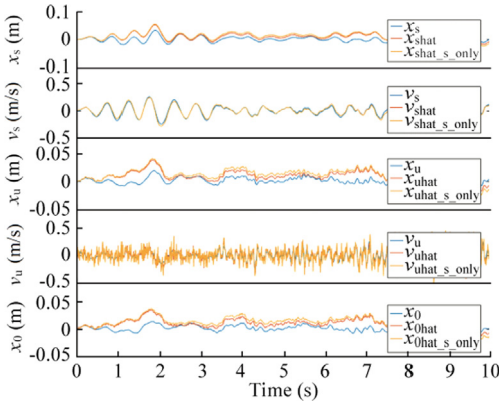

Fig. 5. Estimated states from the simulated data set. As seen, velocities are well estimated, while positions are drifting slightly. The high frequency behavior of the road profile is very well estimated.

This shows that as long as the data-generation process is similar enough to a quarter car model with correct parameters, and there is sufficient signal to (Gaussian) noise ratio, the quarter car model can be used in reverse to estimate road profiles from acceleration data. If this assumption does not hold, we can say little about the accuracy of the approach.

The quarter car model can thus in simulation be shown to work in reverse together with a Kalman filter, given that the wheel suspension can be accurately described by a quarter car model. However, running experimental data through the quarter car Kalman filter of the pick-up truck running over a wooden board at various speeds did not produce results in line with the simulation. Fig. 6 shows the estimated parameters as the pick-up truck passes a known size wooden board. A perfect filter algorithm would show a 45 mm × 75 mm rectangular obstacle at t = 10 s, t = 28 s, and t = 45 s, which is clearly not the case. The effect is visible; however, the road profile is not well estimated.

The quarter car model is thus effective in simulation, but not on our experimental data. If the quarter car model is indeed a suitable

Please cite this article as: M. Åstrand, E. Jakobsson, M. Lindfors et al., A system for underground road condition monitoring, International Journal of Mining Science and Technology, https://doi.org/10.1016/j.ijmst.2020.04.006

model for the wheel suspension, the reason for this discrepancy could be due to the model parameters. The exact value for spring stiffness, suspension weight and tire stiffness could not be experimentally determined during the project, and rough estimates were used, which could explain the resulting difference between simulations and real data. Whether the model parameters or the model structure is the root cause is currently unknown. To fully verify if a quarter car model is an appropriate approximation for this particular vehicle, a more controlled experiment using laser-scanned road profiles and known vehicle parameters would be required.

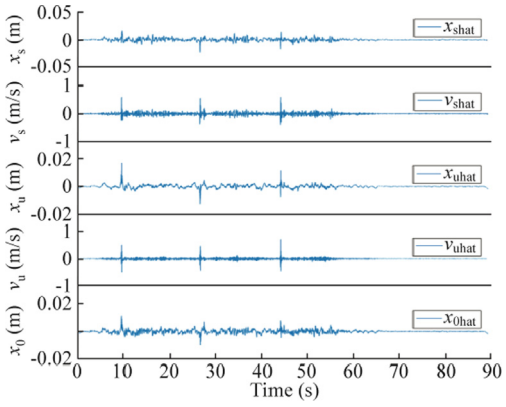

Fig. 6. Estimated states from passing a 45 mm wooden board in 20 km/h at t = 10 s, t = 28 s, and t = 45 s.

Fig. 7. Final positioning and road condition results. Colors indicate a relative road roughness measure based on spectral energy, where blue is smooth and red is quite bumpy.

Due to performance setbacks using a quarter car Kalman approach on experimental data, the power spectral density is used to estimate a relative measure on the roughness of the road for combination with the localization results. The PSD is calculated using a hamming window of 50 samples, resulting in a time resolution of 0.25 s. The vehicle velocity has a large influence on the amount of energy in the vibrations signals, so following [19] the PSD value is compensated by dividing with the velocity squared to have similar power levels for different velocities. This relation was also verified by data acquired from passing identical obstacles at a number of different speeds.

The results of a test drive combining both the localization of the vehicle and the road condition index are visualized in Fig. 7, providing a map of the road condition in the ramp. Colors are used to indicate the road condition index, where red is the roughest measurements, blue the smoothest and a spectral scale in between.

3.3. Rescheduling

The red parts in Fig. 8 indicate relatively ill-conditioned road segments. To be able to automatically respond to this information, the constraint program presented in Section 2.3 is implemented in Gecode [20], where generated instances are solved on a laptop with an i7-7500U processor and 16 GB RAM. Additional input data to the scheduling problem e.g. the number of active faces, machines of each type, and task durations, are parameters given by the mine operators.

A short-term production schedule can be seen in Fig. 9a, where a total of 110 tasks are scheduled on 10 different faces. The color coding of the activities indicates what type of machinery is needed to perform the activity. The red rectangle corresponds to a potential additional constraint added by the road service disturbance: once a task has started on adjacent faces it may continue, but no new tasks can start. This is modeled by

$$s^f_{ir} < t_{\text{start}} \vee s^f_{ir} > t_{\text{end}} \ \forall (i,r,f) \text{s.t. } f \in [0,3] \tag{31}$$

where $t_{\text{start}} \approx 27$ h and $t_{\text{end}} \approx 33$ h.

A revised feasible schedule using the rescheduling algorithm described in Section 2.3.2 can be seen in Fig. 9b. It appears that LNS with a growing time-based relaxation can be a beneficial method for finding a new schedule that resembles the original schedule. As a comparison, solving for a completely new schedule under the road service disturbance can be seen in Fig. 9c. By section, using such a naive rescheduling strategy creates more changes between the original schedule and new schedule.

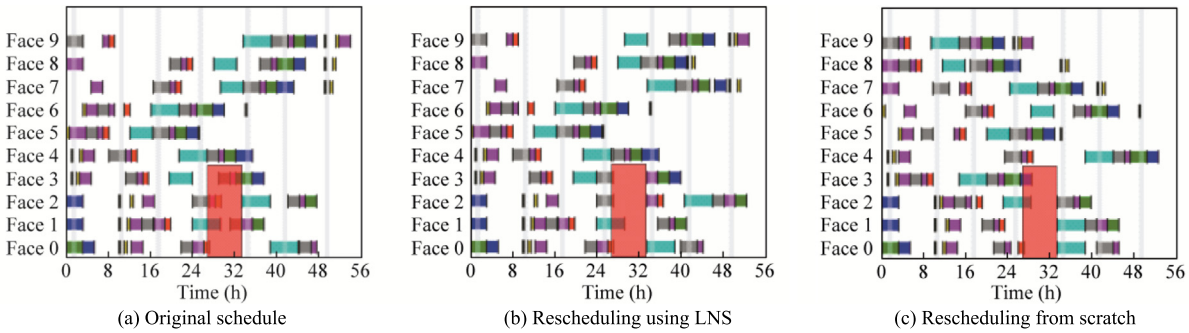

(a) Original schedule (b) Rescheduling using LNS (c) Rescheduling from scratch

Fig. 8. A short-term schedule of the production machines (a). The red rectangle corresponds to the additional availability constraints inferred by a road service activity. Note that rescheduling using a time-based relaxation window creates a revised schedule (b) that resembles the original schedule (a). For comparison, (c) shows a completely new schedule adhering to the additional service constraints.

Please cite this article as: M. Åstrand, E. Jakobsson, M. Lindfors et al., A system for underground road condition monitoring, International Journal of Mining Science and Technology, https://doi.org/10.1016/j.ijmst.2020.04.006

4. Conclusions

Bad road conditions may lead to increased wear on vehicles and limit the pace of production. In this work, a proof-of-concept road condition monitoring system for underground mining has been demonstrated. The system is based on localizing vehicles using onboard sensors and signal strength from the existing WiFi production network. Two methods for road condition estimation were introduced, where a quarter car model works well in simulation, but a system based on power spectral density is more easily applied to experimental data. To be able to act automatically on poor road conditions, a rescheduling strategy was detailed accommodating for road service disturbances. A proof-of-concept demonstration of the joint system on experimental data from a Swedish underground mine shows promising results.

Future work includes improving the initialization procedure by extending the RSS model to, for instance, consider that signal strength deteriorates more rapidly in curves. Further, a benefit of the quarter-car condition monitoring approach is that it enables wear calculations for a wide range of different vehicles. However, to work on experimental data, a more detailed vehicle model and better parameter estimates are likely needed. Lastly, for the rescheduling algorithm, it would be interesting to study different structured relaxations that represent other maintenance scenarios.

Declaration of Competing Interest

The authors declare that they have no known competing financial interests or personal relationships that could have appeared to influence the work reported in this paper.

Acknowledgements

All authors are partially supported by the Wallenberg AI, Autonomous Systems and Software Program (WASP) funded by the Knut and Alice Wallenberg Foundation. The authors gratefully acknowledge the assistance of Boliden Kankberg and Mobilaris in the experiments.

References

[1] Forooshani AE, Bashir S, Michelson DG, Noghanian S. A survey of wireless communications and propagation modeling in underground mines. IEEE Commun Surv Tutor 2013;15(4):1524–45.
[2] Zlot R, Bosse M. Efficient large-scale three-dimensional mobile mapping for underground mines. J Field Rob 2014;31(5):758–79.
[3] Chatti K, Zaabar I. Estimating the effects of pavement condition on vehicle operating costs. Transp Res Board 2012.
[4] Brickman AD, Wambold JC, Zimmerman JR. An amplitude-frequency description of road roughness. Highway Res Board Special Rep 1971;116:53–67.
[5] Song Z, Schunnesson H, Rinne M, Sturgul J. Intelligent scheduling for underground mobile mining equipment. PLoS ONE 2015;10(6):e0131003.
[6] Schulze M, Rieck J, Seifi C, Zimmermann J. Machine scheduling in underground mining: an application in the potash industry. OR Spectrum 2016;38(2):365–403.
[7] Shaw P. Using constraint programming and local search methods to solve vehicle routing problems. In: Proceedings of international conference on principles and practice of constraint programming. Berlin: Springer; 1998. p. 417–31.
[8] Dorn J. Case-based reactive scheduling. Boston (MA): Springer; 1995. p. 32–50.
[9] Fossen TI. Guidance and control of ocean vehicles. John Wiley & Sons Inc; 1994.
[10] Huber PJ. Robust statistics. Springer; 2011.
[11] Doucet A, Godsill S, Andrieu C. On sequential Monte Carlo sampling methods for Bayesian filtering. Stat Comput 2000;10(3):197–208.
[12] Sayers MW. The international road roughness experiment: establishing correlation and a calibration standard for measurements. Ann Arbor: University of Michigan; 1986.
[13] Kalman RE. A new approach to linear filtering and prediction problems. J Fluids Eng, Trans ASME 1960;82(1):35–45.
[14] Särkkä S. Bayesian filtering and smoothing. Cambridge University Press; 2013.
[15] Welch PD. The use of fast fourier transform for the estimation of power spectra: a method based on time averaging over short, modified periodograms. IEEE Trans Audio Electroacoust 1967;15(2):70–3.
[16] Baptiste P, Le Pape C. Nuijten W. Constraint-based scheduling: applying constraint programming to scheduling problems. Springer Science & Business Media; 2012.
[17] Laborie P, Rogerie J. Reasoning with conditional time-intervals. In: Proceedings of the 21st international Florida artificial intelligence research society conference, FLAIRS-21. Coconut Grove (FL); 2008. p. 555–60.
[18] Åstrand M, Johansson M, Zanarini A. Fleet scheduling in underground mines using constraint programming. In: Proceedings of the 15th international conference on integration of constraint programming, artificial intelligence, and operations research, CPAIOR 2018. Delft: Springer Verlag; 2018. p. 605–13.
[19] Alessandroni G, Carini A, Lattanzi E, Freschi V, Bogliolo A. A study on the influence of speed on road roughness sensing: The smartroadsense case. Sensors (Switzerland) 2017;17(2):305.
[20] Schulte C, Lagerkvist M, Tack G. Gecode: Generic constraint development environment. Proceedings of INFORMS annual meeting, 2006.

Please cite this article as: M. Åstrand, E. Jakobsson, M. Lindfors et al., A system for underground road condition monitoring, International Journal of Mining Science and Technology, https://doi.org/10.1016/j.ijmst.2020.04.006